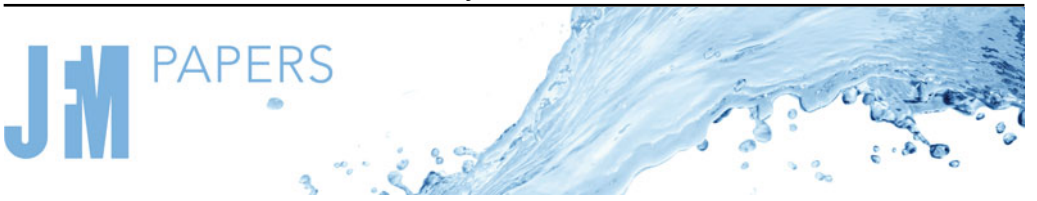
*J. Fluid Mech.* (2026), *vol.* 1035, A10, doi:10.1017/jfm.2026.11535




# Quantifying the surface layer generated by strong free-surface turbulence

**Declan B. Gaylo**[1] **and Dick K.P. Yue**[1]

[1]Department of Mechanical Engineering, Massachusetts Institute of Technology, Cambridge, MA 02139, USA

**Corresponding author:** Dick K.P. Yue, yue@mit.edu

(Received 23 December 2025; revised 6 March 2026; accepted 7 April 2026)

We consider free-surface flows driven by turbulence beneath the surface, particularly the strong free-surface turbulence (FST) regime, characterised by large Froude number $Fr_T^2 = \varepsilon/u_{rms}g \gtrsim 0.1$. We study the surface layer, where air and water are highly mixed and turbulence modelling is challenging. We develop a definition of the surface-layer thickness $\delta_s$ based on the vertical derivative of intermittency $\gamma$ at the mean free surface $\bar{\eta}$, which, unlike previous definitions, is independent of the tail behaviour of $\gamma$. From direct numerical simulation (DNS) of statistically stationary, horizontally homogeneous strong FST, we show that scaling by $z^* = (z - \bar{\eta})/\delta_s$ collapses $\gamma$ across a wide range of $Fr_T^2 \in [0.03, 0.3]$. The distribution more closely follows logistic rather than Gaussian behaviour. From the near-surface turbulence obtained from DNS, we make two general observations. First, we show that for strong FST there is minimal direct effect of the free surface on the isotropy, turbulence kinetic energy $\tilde{k}$ or dissipation rate $\varepsilon$ beneath the surface layer ($z^* < -0.5$). Instead, turbulence is only indirectly affected through the flux of kinetic energy into the surface layer. Second, we show that many relevant metrics within the surface layer ($z^* \in [-0.5, 0.5]$) collapse when appropriately scaled by $u_{rms}^2 = 2\tilde{k}/3$ and $\varepsilon$ measured at $z^* = -0.5$. These observations suggest the possibility of a turbulence closure model which avoids direct modelling of $\tilde{k}$ and $\varepsilon$ in the surface layer. Towards this, we show that, across a wide range of $Fr_T^2$, surface-layer thickness can be predicted by $\delta_s \approx 11.1\, u_{rms}^2 g^{-1}$ and energy flux into the surface layer by $W \approx 0.41\, \varepsilon\delta_s$.

**Key words:** interfacial flows (free surface), gas/liquid flow, turbulent flows

## 1. Introduction

Turbulence beneath an air–water free surface is present in a large variety of natural and engineering flows. In many of these flows – e.g. dam spillways, rivers (Chanson 1996) and ship wakes (Hendrickson *et al.* 2019) – this free-surface turbulence (FST) is strong

© The Author(s), 2026. Published by Cambridge University Press.



https://doi.org/10.1017/jfm.2026.11535 Published online by Cambridge University Press

relative to the restoring forces of gravity and surface tension, causing the free surface to be broken up (Brocchini & Peregrine 2001*a*). A highly visible feature of these flows is the creation of bubbles and droplets, with the former leading these strong FST flows being also referred to as self-aerating flows or air-entraining flows. Predicting the quantity and size distribution of bubbles in these flows is of interest, and many of the mechanisms that shape the bubble population are the direct result of near-surface turbulence – e.g. bubble fragmentation (Hinze 1955; Martínez-Bazán *et al.* 1999; Qi *et al.* 2022) and bubble entrainment (Zabaleta, Bombardelli & Márquez Damián 2024; Gaylo & Yue 2025). In this work we focus on characterising the turbulence near the surface in air-entraining FST.

An important quantity for characterising FST is the turbulent Froude number $Fr_T^2 = \varepsilon/u_{rms}g$, where dissipation rate $\varepsilon$ and turbulence fluctuations $u_{rms}$ are measured near the surface. This quantity compares the disturbing effect of near-surface turbulence on the free surface to the restoring effect of gravity. For $Fr_T^2 \ll 1$ the free surface is only slightly deformed and there is a blockage effect, with vertical turbulent fluctuations near the surface being suppressed (Shen *et al.* 1999; Guo & Shen 2010; Ruth & Coletti 2024). For large $Fr_T^2$, the blockage effect weakens and vertical turbulent fluctuations break apart the free surface (Yu *et al.* 2019; Calado & Balaras 2025; Gaylo & Yue 2025). In place of a continuous free surface is a region where water and air are highly mixed, called the surface layer. Due to the highly variable density in this surface layer, turbulence modelling is a challenge (Brocchini & Peregrine 2001*a*; Hendrickson & Yue 2019).

One air-entraining turbulent flow which is often studied is supercritical open-channel flow (Chanson 1996). An approach to modelling the boundary-layer turbulence in this flow is to separately model the surface layer (referred to as turbulent wavy layer) and the turbulent boundary layer beneath (Killen 1968; Kramer & Valero 2023). We note that in these flows there is typically not a large separation of scales: the size of the surface layer is similar to the total depth of the flow. This implies a close relationship between the dynamics in the surface layer and the turbulent boundary layer beneath, making it a challenge to generalise models for open-channel flow to other free-surface flows. Studying free-surface wakes, Hendrickson *et al.* (2019) note that the resulting air-entraining FST bears little similarity to open-channel flow. For free-surface flows in general, Brocchini & Peregrine (2001*b*) provide a theoretical framework for modelling the surface layer based on phase-weighted averaging. For the case where the surface layer is thin relative to the large-scale features of the flow, Brocchini (2002) shows theoretically how the surface layer could be treated as a modified boundary condition in $k$–$\varepsilon$ type Reynolds-averaged Navier–Stokes (RANS) simulations. Even for flows where the thin-surface-layer assumption is weak, this modelling approach can be valuable; Iravani, Badiei & Brocchini (2020) show it improves RANS predictions of near-surface turbulent kinetic energy in breaking waves.

Different air-entraining FST flows have different mechanisms that generate turbulence in the water. We consider air-entraining FST where the mechanisms that generate turbulence in the water are sufficiently separate (in either distance or scale) from the surface layer such that the turbulence statistics near the surface layer have a universal character independent of the specifics of the generating mechanisms. We perform direct numerical simulation (DNS) of a canonical example of such a flow, where homogeneous, statistically steady turbulence is generated in a region deep beneath the free surface (Guo & Shen 2009; Calado & Balaras 2025; Gaylo & Yue 2025). In § 2 we develop a quantitative definition of the surface-layer thickness $\delta_s$, which, unlike previous definitions (Brocchini & Peregrine 2001*b*), is independent of the quantity of bubbles deep beneath the surface and makes no assumptions about the distribution of intermittency $\gamma$, which is defined as the mean portion of volume occupied by water. In § 4, using measurements from DNS across a wide range of $Fr_T^2$, we quantify the distribution of intermittency, confirming that it collapses with $Fr_T^2$



https://doi.org/10.1017/jfm.2026.11535 Published online by Cambridge University Press

after scaling by $\delta_s$ and showing that it generally follows a logistic distribution. In § 5 we study the turbulence in the surface layer and find that for strong FST where near-surface turbulence is isotropic ($Fr_T^2 > 0.1$), the turbulence within the surface layer only depends on $\delta_s$ and the turbulence quantities at the bottom of the surface layer. These results confirm the possibility of modelling the surface layer as a modified boundary condition in RANS, especially for strong FST. In § 6 we show how the surface-layer thickness $\delta_s$ and the work done on the surface layer $W$ scale with $Fr_T^2$. These are the two quantities necessary for such a boundary condition.

## 2. Defining the surface layer in FST

The defining property of the surface layer is the heterogeneous mixture of two fluids, here air and water. At any instant, this mixture can be described by a binary colour function field:

$$c(\boldsymbol{x}, t) \equiv \begin{cases} 0 & \text{if} \quad \boldsymbol{x} \in \text{air} \\ 1 & \text{if} \quad \boldsymbol{x} \in \text{water}. \end{cases} \tag{2.1}$$

Our interest is the average behaviour of the surface layer, and we consider the simplest case where FST is horizontally and temporally homogeneous. We use an average along the homogeneous dimensions,

$$\overline{\cdot} \equiv \frac{\iiint \cdot \, \mathrm{d}x \, \mathrm{d}y \, \mathrm{d}t}{\iiint \mathrm{d}x \, \mathrm{d}y \, \mathrm{d}t}, \tag{2.2}$$

to define the intermittency factor

$$\gamma(z) \equiv \overline{c(\boldsymbol{x}, t)}, \tag{2.3}$$

which here is only a function of depth $z$. This intermittency factor gives the average portion of volume occupied by water, with $\gamma = 1$ corresponding to all water and $\gamma = 0$ to all air (Brocchini & Peregrine 2001*b*). The opposite, $1 - \gamma$, is the void fraction.

Because the free surface is highly distorted, we first need a definition of the mean free surface. While alternative definitions may be more appropriate for wave-driven flows (Brocchini & Peregrine 1996, 2001*b*), for FST we find a simple definition is sufficient. We define the mean free-surface height $\bar{\eta}$ as the height where air and water are evenly mixed:

$$\gamma(z = \bar{\eta}) = 0.5. \tag{2.4}$$

We note that, because FST entrains air bubbles deep beneath the free surface, $\bar{\eta}$ will be higher than the location of the quiescent free surface. In this way, $\bar{\eta}$ is a measure of bubble entrainment, which is the focus of Gaylo & Yue (2025). Our interest here is the turbulence near the free surface rather than bubbles deep beneath, so we focus on the depth relative to $\bar{\eta}$, $z - \bar{\eta}$.

Because the defining characteristic of the surface layer is mixing of air and water, it is common to choose $\gamma_{max}$ and $\gamma_{min}$, and define the surface layer as the depths $z$ where $\gamma_{max} > \gamma(z) > \gamma_{min}$ (Brocchini & Peregrine 2001*b*). Hendrickson & Yue (2019) express this in terms of density $\rho_{max} > \overline{\rho}(z) > \rho_{min}$, which is equivalent. The choice of these limits is somewhat arbitrary. To justify a choice, Brocchini & Peregrine (2001*b*) start by considering a single-valued free surface where instantaneous free-surface height $\eta(x, y, t)$ follows a Gaussian distribution with mean $\bar{\eta}$ and variance $\sigma^2$. It can be shown that this



https://doi.org/10.1017/jfm.2026.11535 Published online by Cambridge University Press

gives an intermittency factor

$$\gamma_{Gaussian}(z) = \frac{1}{2}\left[1 - \mathrm{erf}\left(\frac{z-\bar{\eta}}{\sqrt{2}\sigma}\right)\right]. \tag{2.5}$$

Using $z-\bar{\eta} \in [-3\sigma, 3\sigma]$ to define the surface layer gives $\gamma_{min} \approx 0.001$ and $\gamma_{max} \approx 0.999$. In § 4 we show that FST produces a non-negligible volume of bubbles deep beneath the free surface, causing a non-Gaussian distribution, where $\gamma$ approaches 1 very slowly. Due to these bubbles, we find $\gamma_{max} \approx 0.999$ overestimates the depth of the surface layer. More generally, a challenge with using $\gamma_{max}$ and $\gamma_{min}$ is that the resulting definition of the surface layer depends on the tail behaviour of $\gamma$, which may be only indirectly linked to the behaviour close to the mean free surface.

As a more robust definition of the surface layer, we use the behaviour of $\gamma$ at the mean free surface rather than the tail behaviour far from the mean free surface. To do this, we define a free-surface thickness in terms of the vertical derivative of $\gamma$ evaluated at the mean free surface $\bar{\eta}$:

$$\delta_s \equiv C_{\mathrm{d}\gamma}\left(\left.\frac{\mathrm{d}\gamma}{\mathrm{d}z}\right|_{z=\bar{\eta}}\right)^{-1}. \tag{2.6}$$

Asserting that the surface layer is centred about $\bar{\eta}$, depths $z-\bar{\eta} \in [-\delta_s/2, \delta_s/2]$ define the surface layer. For characterising depth relative to the surface layer, we define a non-dimensionalised depth,

$$z^* \equiv \frac{z-\bar{\eta}}{\delta_s}, \tag{2.7}$$

in which case the surface layer is non-dimensional depths $z^* \in [-0.5, 0.5]$.

What remains in (2.6) is to determine the constant $C_{\mathrm{d}\gamma}$ such that $\delta_s$ does a good job in characterising the surface layer. To start, we choose the constant $C_{\mathrm{d}\gamma} = 6/\sqrt{2\pi}$ so that in the case where $\gamma = \gamma_{Gaussian}$, $\delta_s = 6\sigma$ and our definition of the surface layer is equivalent to $z-\bar{\eta} \in [-3\sigma, 3\sigma]$ from Brocchini & Peregrine (2001*b*). While initially somewhat arbitrary, it turns out that $C_{\mathrm{d}\gamma} = 6/\sqrt{2\pi}$ is an appropriate choice. Using DNS of FST at a wide range of turbulent Froude numbers $Fr_T^2$, we show in §§ 4 and 5 that the resulting $\delta_s$ indeed characterises the surface layer. Specifically, scaling by $z^*$ and turbulence properties measured at the bottom of the surface layer, $z^* = -0.5$, collapses measurements in the surface layer across a wide range of $Fr_T^2$; and $z^* = -0.5$ is appropriate to separate the surface layer where turbulence is directly affected by the free surface from the region beneath where turbulence is only indirectly affected. These two insights suggest the possibility of distinct turbulence closure modelling within the surface layer, and in § 6 we show how $\delta_s$ can be predicted *a priori*.

## 3. Direct numerical simulation of statistically steady FST

To study FST, we pick a flow which isolates FST from other free-surface mechanisms (e.g. waves) and is homogeneous in the horizontal and temporal dimensions. This flow is a forced free-surface turbulence, where isotropic turbulence is continuously forced deep beneath the surface to obtain statistically steady turbulence at the surface. Simulations of this flow were first performed by Guo & Shen (2009) for $Fr_T^2 \ll 1$, and have recently been extended to moderate and large $Fr_T^2$ (Calado & Balaras 2025; Gaylo & Yue 2025). In this work, we analyse the simulations from Gaylo & Yue (2025) and perform additional simulations to obtain even larger $Fr_T^2$ (see table 1). For completeness, we summarise the



https://doi.org/10.1017/jfm.2026.11535 Published online by Cambridge University Press

| | $g^{-1}$ | $\nu_w^{-1}$ | $\bar{\eta}$ | $\delta_s$ | $u_{rms}$ | $\varepsilon$ | $\ell$ | $Fr_T^2$ | $Re_T$ |
|---|---|---|---|---|---|---|---|---|---|
| GY25, a.i | 0.3 | 200 | 0.010 | 0.41 | 0.27 | 0.025 | 0.81 | 0.03 | 44 |
| GY25, a.ii | 0.6 | 200 | 0.030 | 0.77 | 0.30 | 0.030 | 0.89 | 0.06 | 53 |
| GY25, a.iii | 0.9 | 200 | 0.080 | 1.08 | 0.34 | 0.030 | 1.32 | 0.08 | 90 |
| GY25, a.iv | 1.2 | 200 | 0.124 | 1.29 | 0.27 | 0.030 | 0.69 | 0.13 | 38 |
| New | 1.5 | 200 | 0.180 | 1.40 | 0.27 | 0.028 | 0.73 | 0.15 | 40 |
| GY25, a.v | 1.8 | 200 | 0.268 | 1.60 | 0.30 | 0.030 | 0.85 | 0.18 | 50 |
| New | 2.1 | 200 | 0.345 | 1.73 | 0.27 | 0.027 | 0.70 | 0.21 | 37 |
| New | 2.4 | 200 | 0.363 | 1.78 | 0.26 | 0.024 | 0.74 | 0.22 | 39 |
| New | 2.7 | 200 | 0.543 | 1.76 | 0.26 | 0.024 | 0.69 | 0.26 | 35 |

Table 1. For simulations from Gaylo & Yue (2025) (GY25), the labels used in that paper are provided. All values are non-dimensionalised by the characteristic turbulent scales in the forcing region. Turbulence properties $u_{rms}$ and $\varepsilon$ are measured at the bottom of the surface layer ($z^* = -0.5$). The characteristic length scale $\ell = u_{rms}^3/\varepsilon$ is used to calculate the near-surface turbulent Froude number $Fr_T^2 = (u_{rms}^2/\ell)/g$ and the turbulent Reynolds number $Re_T = (u_{rms}\ell)/\nu_w$.

simulations from Gaylo & Yue (2025) and note the small change needed for the new, larger-$Fr_T^2$ simulations.

We perform DNS by solving the three-dimensional incompressible Navier–Stokes equation for two immiscible phases:

$$\frac{\partial \rho \boldsymbol{u}}{\partial t} + \boldsymbol{u}\cdot\boldsymbol{\nabla}\,(\rho \boldsymbol{u}) = -\boldsymbol{\nabla} p + \boldsymbol{\nabla}\cdot\boldsymbol{\tau} - \rho g \hat{\boldsymbol{e}}_z + \rho \boldsymbol{f}, \tag{3.1a}$$

$$\boldsymbol{\nabla}\cdot\boldsymbol{u} = 0, \tag{3.1b}$$

$$\frac{\partial c}{\partial t} + \boldsymbol{u}\cdot\boldsymbol{\nabla} c = 0, \tag{3.1c}$$

where $\boldsymbol{\tau} = \mu(\boldsymbol{\nabla}\boldsymbol{u} + \boldsymbol{\nabla}\boldsymbol{u}^{\mathrm{T}})$ is the viscous stress tensor. Numerically, we solve these equations on a uniform Cartesian grid using a second-order finite-volume scheme (Campbell 2014; Yu *et al.* 2019). In (3.1*a*) all terms but pressure are treated explicitly, and the pressure projection method is used to solve for pressure and satisfy (3.1*b*). For (3.1*c*), we use the conservative volume-of-fluid method, which maintains a sharp interface between air and water and ensures volume conservation of both to machine precision (Weymouth & Yue 2010). Density is given by

$$\rho \equiv \rho_a c + (1-c)\rho_w, \tag{3.2}$$

and similar for viscosity $\mu$. We use realistic air–water values of $\rho_a/\rho_w = 0.00123$ and $\mu_a/\mu_w = 0.0159$. To focus on the scaling with $Fr_T^2$ rather than Weber number $We$, we neglect surface tension, in effect setting $We = \infty$. While this means that the behaviour of small, sub-Hinze-scale bubbles is not resolved (Hinze 1955; Ruth *et al.* 2022), studies of this flow including surface tension have confirmed that its effect on turbulence and large bubbles is small for large Froude and Weber numbers (Calado & Balaras 2025; Gaylo & Yue 2025).

To obtain statistically steady turbulence, energy is added deep beneath the free surface through linear forcing (Lundgren 2003; Rosales & Meneveau 2005), where $\boldsymbol{f} = A\boldsymbol{u}' F_b(z_c)$ and

$$F_b(z_c) = \begin{cases} 0 & z_c > l_b + l_d \\ \dfrac{1}{2}\left(1 - \cos\left[\dfrac{\pi}{l_d}(z_c - l_b - l_d)\right]\right) & z_c \le l_b + l_d \\ 1 & z_c \le l_b \end{cases} \tag{3.3}$$



https://doi.org/10.1017/jfm.2026.11535 Published online by Cambridge University Press

keeps the forcing primarily in a forcing region of height $2l_b = 3\pi$ centred around $z_c$. Using the method described by Rosales & Meneveau (2005), the value of $A$ is chosen dynamically to give characteristic turbulent scales of unity ($\varepsilon$ and $u_{rms} = 1$) within this forcing region. There are damping regions $l_d = \pi/2$ on either side of the forcing region, then a free length $l_f = \pi/2$ before the bottom of the domain or the quiescent free surface at $z = 0$. Gaylo & Yue (2025) use an air gap of height $\pi$ above the quiescent free surface. For the larger-$Fr_T^2$ simulations performed in this work ($g^{-1} > 2$), the air gap was increased to $1.75\pi$ to avoid the top boundary affecting the turbulence. The horizontal domain length is $2\pi$. Gaylo & Yue (2025) show that a $256^2 \times 768$ grid resolves the Kolmogorov microscale ($\eta_T/\Delta \approx 1.8$ near the surface), and our increased air gap makes the grid $256^2 \times 864$. After the simulation has reached a statistically steady state, 400 evenly spaced samples over 128 eddy turnover times $u_{rms}^2/\varepsilon$ (based on turbulence in the forcing region, $\varepsilon$ and $u_{rms} = 1$) are used for the temporal averaging in (2.2).

Our interest is the turbulence levels near the surface, so it is useful to define non-dimensional numbers based on the near-surface turbulence. At $z^* = -0.5$, we measure the turbulence kinetic energy

$$\overline{\rho}\tilde{k} \equiv \overline{\frac{1}{2}\rho \boldsymbol{u} \cdot \boldsymbol{u}}, \tag{3.4}$$

which gives a characteristic velocity $u_{rms} = \sqrt{2\tilde{k}/3}$, and the dissipation rate

$$\overline{\rho}\varepsilon \equiv \overline{\tau_{ij}\, \partial u_i/\partial x_j}. \tag{3.5}$$

These measurements are shown in table 1, and are used to define near-surface non-dimensional numbers. Most relevant here is turbulent Froude number $Fr_T^2 = \varepsilon/u_{rms}g$. We note that using the turbulence levels at $z^* = -0.5$ gives only slightly different non-dimensional numbers from those using a near-surface water-phase average (Gaylo & Yue 2025, (3.4)). In § 5 we show that the turbulence levels at $z^* = -0.5$ best characterise the turbulence within the surface layer.

## 4. Intermittency in the surface layer

From the DNS results, we start by analysing the intermittency factor $\gamma(z)$. Figure 1 shows $\gamma(z)$ for the range of $Fr_T^2$, before and after scaling relative depth $z - \bar{\eta}$ by $\delta_s$. Given that $\delta_s$ is defined by the derivative of $\gamma$ at $z = \bar{\eta}$, the distributions necessarily collapse at the mean free surface. However, we also see that scaling by $\delta_s$ also does a good job in collapsing the distribution of $\gamma(z)$ throughout the surface layer. For $z^* < -0.5$ we do see some small $Fr_T^2$-dependent differences, and in § 4.1 we confirm that these are almost entirely the result of $Fr_T^2$-dependent bubble entrainment rates. In § 4.2 we investigate the shape of $\gamma(z)$ and show that it is closer to a logistic distribution than to the Gaussian distribution discussed by Brocchini & Peregrine (2001*b*).

### 4.1. *Separating out the effects of bubbles and droplets*

The intermittency factor $\gamma$ includes the effects of three different types of features: the free surface, bubbles and droplets. To separate these, we start by applying a connected component-labelling algorithm (Hendrickson, Weymouth & Yue 2020) to identify contiguous regions of air that are disconnected from the bulk region of air above the free surface (bubbles) and contiguous regions of water that are disconnected from the bulk region of water below the free surface (droplets). From this post-processing, we define



https://doi.org/10.1017/jfm.2026.11535 Published online by Cambridge University Press

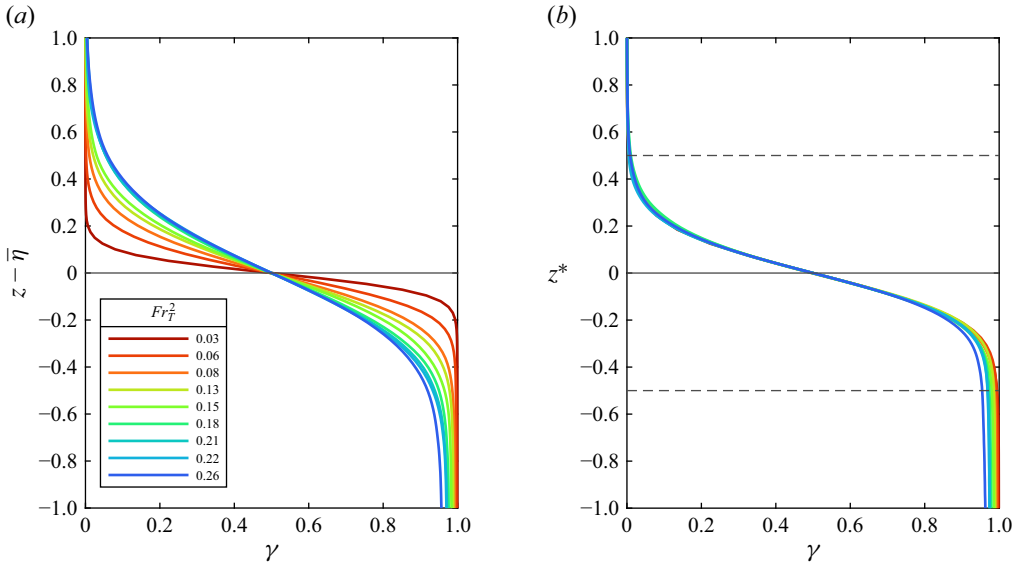



Figure 1. Intermittency factor $\gamma$ as a function of (*a*) height relative to the mean free surface and (*b*) height scaled by surface-layer thickness. Solid curves indicate the mean free surface $\bar{\eta}$ and in (*b*) dashed lines show the extent of the surface layer.

two new binary colour functions:

$$c_D(\boldsymbol{x}, t) \equiv \begin{cases} 1 & \text{if } \boldsymbol{x} \in \text{droplet of water} \\ 0 & \text{otherwise;} \end{cases} \tag{4.1a}$$

$$c_B(\boldsymbol{x}, t) \equiv \begin{cases} -1 & \text{if } \boldsymbol{x} \in \text{bubble of air} \\ 0 & \text{otherwise.} \end{cases} \tag{4.1b}$$

Subtracting these from the original colour function, we obtain a third binary colour function:

$$c_0 \equiv c - (c_D + c_B), \tag{4.1c}$$

which describes the mixture of air and water if all bubbles were replaced with water and all droplets replaced with air. This $c_0$ isolates the direct effects of the free surface. Figure 2 shows a representative example of splitting the original colour function $c$ into these three colour functions.

Qualitatively, we note some key differences between figure 2 from DNS (see also the rendering from Gaylo & Yue (2025, figure 3)) and the notional sketch of the surface layer from Brocchini & Peregrine (2001*b*, figure 1). Even for $Fr_T^2$ as high as 0.26, DNS shows that an intact free surface is still easily identifiable. This observation is consistent with experimental work on open-channel flow. While the surface layer appears to the human eye like a uniform mixture of air and water, high-speed photography shows the free surface, while highly distorted, is still mostly intact (Killen 1968; Wilhelms & Gulliver 2005).

To quantify the air–water mixture in the surface layer, we apply averaging like in (2.3) to each of the three new colour functions to obtain $\gamma_0$, $\gamma_B$ and $\gamma_D$, shown in figure 3. These split the intermittency factor into the contributions from each of the three phenomena:

$$\gamma = \gamma_0 + \gamma_B + \gamma_D. \tag{4.2}$$



https://doi.org/10.1017/jfm.2026.11535 Published online by Cambridge University Press

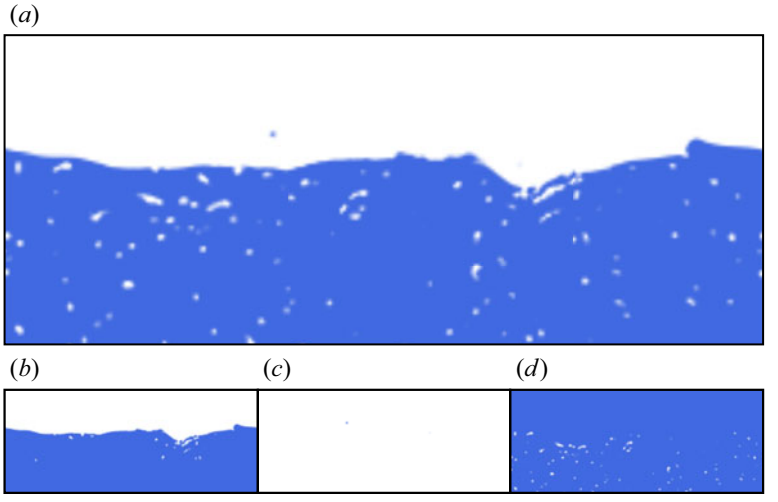



Figure 2. Two-dimensional slice over $z^* \in [-1, +1]$ from the $Fr_T^2 = 0.13$ simulation (GY25, a.iv), showing: (*a*) the original colour function $c$; (*b*) the free-surface colour function $c_0$; (*c*) the droplet colour function $c_D$; and (*d*) the bubble colour function $1 + c_B$. Colour scale from 0 (white) to 1 (blue).

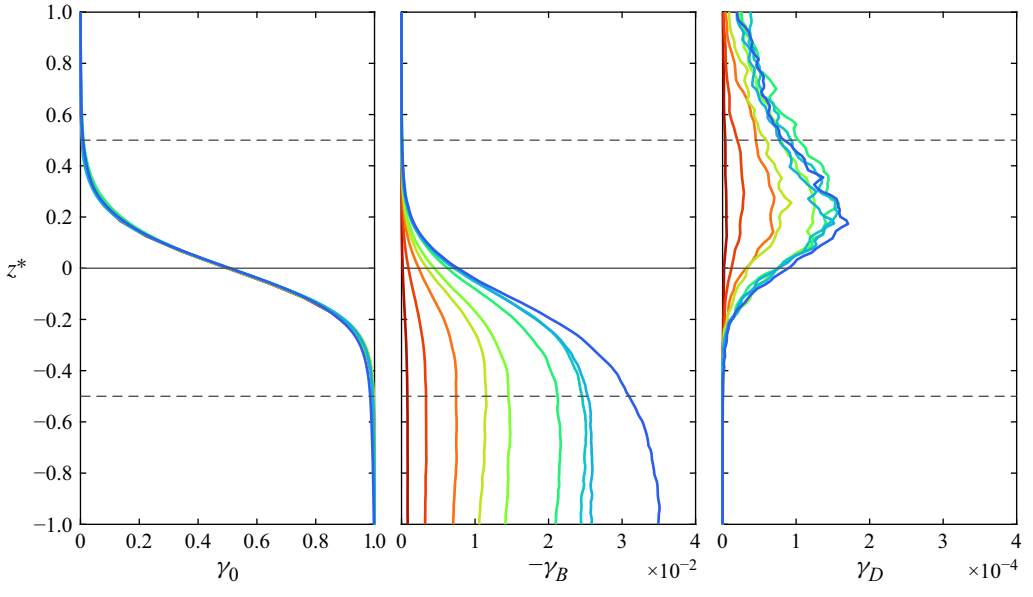



Figure 3. The three subcomponents of intermittency factor $\gamma$ across a range of $Fr_T^2$ (see figure 1*a* for colour legend). Here $\gamma_0$ describes the free surface, $\gamma_B$ bubbles and $\gamma_D$ droplets. Note the difference in magnitude of the horizontal axes.

By rough order of magnitude, we see $\gamma_0$ is 100 times larger than $\gamma_B$, which is 100 times larger than $\gamma_D$. Consistent with the qualitative observations, we see that the effects of the free surface ($\gamma_0$) dominate the surface layer. For droplets, we see a peak in $\gamma_D$ within the upper surface layer ($z^* \approx 0.2$) and then a rapid decay with increasing height. The behaviour for bubbles is very different: $-\gamma_B$ increases with increasing depth throughout the surface layer, and then only very slowly decays with further increasing depth. Because $\rho_a/\rho_w \ll 1$, the mass of a bubble is negligible compared with the water surrounding it, meaning



https://doi.org/10.1017/jfm.2026.11535 Published online by Cambridge University Press

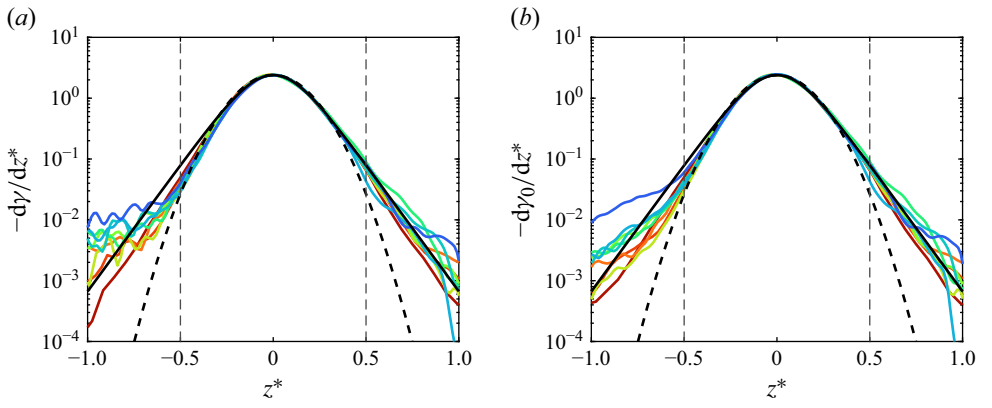



Figure 4. Distribution of (*a*) total intermittency and (*b*) intermittency excluding droplets and bubbles across a range of $Fr_T^2$ (see figure 1*a* for colour legend). Distributions are compared with $\gamma_{Gaussian}$ (small-dashed curves) from (2.5) and $\gamma_{Logistic}$ (black solid curves) from (4.3). Vertical dashed lines show the extent of the surface layer.

that bubble moment is dominated by turbulence in the water rather than the bubble's momentum. For these $Fr_T^2$ where turbulence overcomes the bubble's buoyancy, this means turbulence in the water advects the bubble deep beneath the surface. As expected, $-\gamma_B$ increases with $Fr_T^2$, as bubble entrainment scales like $Fr_T^6$ (Gaylo & Yue 2025).

Focusing on the free-surface effects, we see in figure 3 that the distribution of $\gamma_0$ collapses very well when scaling by $z^*$. Because $\gamma_D$ is so small, droplet effects are negligible. The small-$Fr_T^2$ dependence of $\gamma$ for $z^* < 0$ in figure 1(*b*) is confirmed to be due to the effects of bubbles. For significantly larger bubble void fractions (i.e. larger $Fr_T^2$) one may need to calculate $\delta_s$ using $\gamma_0$ rather than $\gamma$ in (2.6); however, for these simulations the difference is negligible.

### 4.2. *Describing the distribution of intermittency*

We now consider the distribution of the intermittency factor. To highlight the tail behaviour of the distribution, figure 4 shows the derivative of intermittency with $z^*$. Focusing first on $z^* > 0$, we see tail behaviour like $\mathrm{d}\gamma/\mathrm{d}z \propto -\exp[|z|]$. This is opposed to $\mathrm{d}\gamma/\mathrm{d}z \propto -\exp[z^2]$ predicted by (2.5). Instead of Gaussian, this tail behaviour is characteristic of a Logistic distribution:

$$\gamma_{Logistic}(z) = \frac{1}{2}\left[1 - \tanh\left(\frac{z-\bar{\eta}}{s}\right)\right], \tag{4.3}$$

where $s$ is a scale parameter proportional to the standard deviation $\sigma$. The behaviour of $\gamma_0$ (figure 4*b*) is the same as $\gamma$ (figure 4*a*) for $z^* > 0$, demonstrating that this logistic behaviour is the result of free-surface phenomenon rather than droplets. We can compare this result with experiments by Ruth & Coletti (2024), who studied a similar horizontally and temporally steady FST forced from below, but at $Fr_T^2 \ll 1$ where the free surface is not broken. For such a single-valued surface, $-\mathrm{d}\gamma/\mathrm{d}z$ is equivalent to the probability distribution function of free-surface deformations. Their results also appear to follow $\propto \exp[|z|]$ (Ruth & Coletti 2024, figure 5*a*). A physical interpretation of the logistic distribution of $\gamma$ comes from Waclawczyk (2021), who noted analogies between the effects of macroscopic turbulence and mesoscopic thermal fluctuations on intermittency at the respective scales.



https://doi.org/10.1017/jfm.2026.11535 Published online by Cambridge University Press

For $z^* < 0$, the distribution of intermittency is more complicated. Within the lower surface layer ($z^* \in [-0.5, 0]$) it roughly follows a Gaussian distribution; however, beneath the surface layer ($z^* < -0.5$) there is a clear departure and the tail is much larger than predicted by (2.5). While removing the effect of bubbles with $\gamma_0$ reduces the tail, there is still a slow decay compared with (2.5). The logistic distribution does a better job in modelling the tail behaviour, but still does not fully capture it. Physically, the complexity of the tail behaviour can be explained by examining $c_0$ in figure 2(*a*). Even after removing bubbles, there are still pockets of air which, in the two-dimensional slice of the domain, appear separate from the bulk air above the free surface. By moving the location of the two-dimensional slice, we confirm that these are long filaments of air that reach deep beneath the free surface while still being connected to the bulk air above. Long filaments are also evident in the three-dimensional rendering from Gaylo & Yue (2025, figure 3). The filaments are presumably the result of bubbles that recently reconnected to the surface (degassing) or are soon to disconnect from the surface to form a bubble (entrainment), making it rather unclear if filaments should be treated like free-surface phenomena (as done here) or bubble phenomena.

## 5. Turbulence in the surface layer

We now examine the turbulence in and around the surface layer. First, § 5.1 examines the isotropy, confirming that, as noted before (Yu *et al.* 2019; Gaylo & Yue 2025), for sufficient $Fr_T^2$ near-surface turbulence is nearly isotropic. In § 5.2 we examine the terms in the averaged vertical momentum ($\overline{\rho w}$) conservation equation and in § 5.3 the terms in the averaged kinetic energy ($\overline{\rho}\tilde{k}$) conservation equation. Throughout this analysis we show that relevant properties collapse across a wide range of $Fr_T^2$ when properly scaled against $z^*$, and that, partially for strong FST ($Fr_T^2 > 0.1$), the free surface is not felt by the turbulence outside of the surface layer, with $z^* = -0.5$ being the transition point. Later in § 6 we discuss how these insights could be applied to RANS turbulence modelling.

### 5.1. *Isotropy*

For weak FST ($Fr_T^2 \ll 1$), the restoring force of gravity prevents large deformations of the free surface, suppressing vertical fluctuations. This blockage effect creates highly anisotropic turbulence (Shen *et al.* 1999; Guo & Shen 2010; Ruth & Coletti 2024). However, as $Fr_T^2$ increases the strength of the turbulence increases relative to gravity. Yu *et al.* (2019) show that for sufficiently large $Fr_T^2$ the blockage effectively disappears and the near-surface turbulence is nearly isotropic. Calado & Balaras (2025) show that for moderate $Fr_T^2$ vertical fluctuations are partially suppressed. Recently, Gaylo & Yue (2025) proposed $Fr_T^2 = 0.1$ as the approximate transition between moderate FST where vertical fluctuations are partially suppressed and strong FST where the turbulence is nearly isotropic.

To quantify isotropy, we consider the isotropy metric

$$J \equiv 1 - 9\left(\frac{1}{2}b_{ij}b_{ij} - b_{ij}b_{jk}b_{ki}\right), \tag{5.1}$$

where $b_{ij} \equiv \overline{u_i u_j}/\overline{u_k u_k} - \delta_{ij}/3$ is the anisotropy tensor. Here $J = 1$ corresponds to perfectly isotropic turbulence and $J = 0$ corresponds to either one- or two-component turbulence (Pope 2000). Figures 5(*a*) and 5(*b*) show $J$ as a function of depth, unscaled and scaled by $\delta_s$, respectively. Scaling by $\delta_s$ does a good job in collapsing the behaviour of $J$ with depth, and across all $Fr_T^2$ that there is a local minimum in isotropy in the lower surface



https://doi.org/10.1017/jfm.2026.11535 Published online by Cambridge University Press

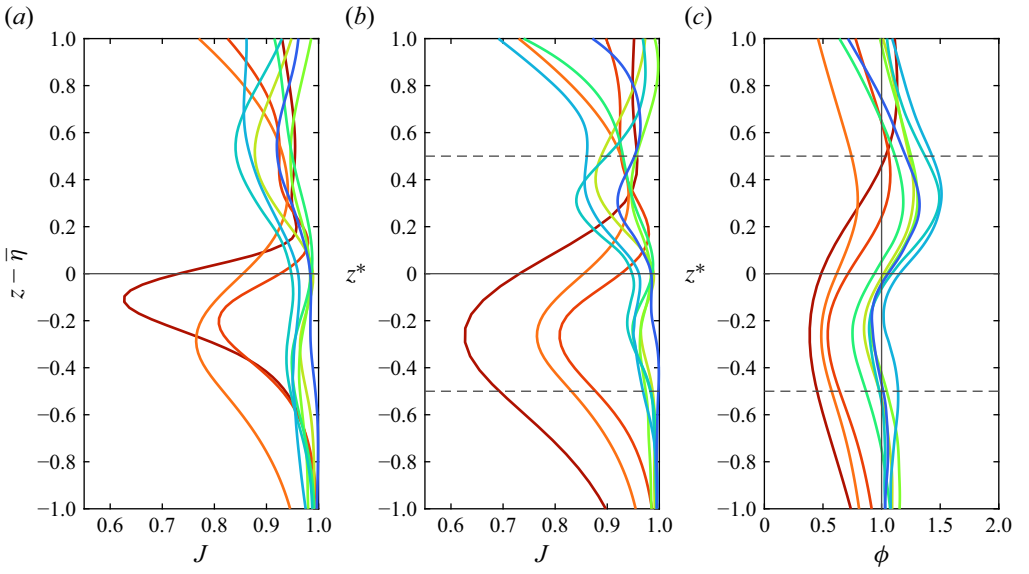



Figure 5. (*a*,*b*) Isotropy metric $J$ and (*c*) relative contributions of vertical fluctuations $\phi$ across a range of $Fr_T^2$ (see figure 1*a* for colour legend).

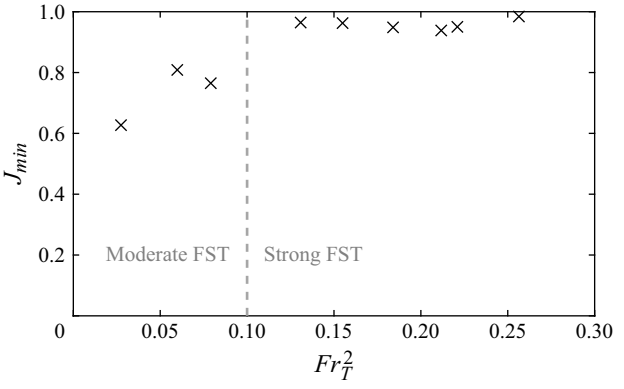



Figure 6. Minimum value of the isotropy metric $J$ in the lower surface layer ($z^* \in [-0.5, 0]$) as a function of $Fr_T^2$, with the approximate transition from moderate to strong FST indicated by the vertical dashed line.

layer, generally at $z^* \approx -0.25$. Figure 6 shows the values of $J$ at these local minimums. As first suggested by Gaylo & Yue (2025), figure 6 confirms a clear transition from moderate FST to strong FST at $Fr_T^2 \approx 0.1$. Returning to figure 5(*b*), we highlight that for strong FST there is not a significant decrease in isotropy until near the bottom of the surface layer ($z^* < -0.5$). This is the first indication that, for strong FST, turbulence beneath the surface layer does not 'feel' the presence of the free surface.

The cause of anisotropy in FST is the effect of gravity on vertical fluctuations, so, to understand $J$, it is useful to consider the relative magnitude of vertical fluctuations,

$$\phi \equiv 3\overline{ww}/\overline{u_k u_k}, \tag{5.2}$$

shown in figure 5(*c*). For moderate FST, we see $\phi < 1$ below and throughout the surface layer, indicating that vertical fluctuations are suppressed. Focusing on strong FST, we see



https://doi.org/10.1017/jfm.2026.11535 Published online by Cambridge University Press

that in the lower surface layer ($z^* \in [-0.5, 0]$) vertical fluctuations are suppressed, but in the upper surface layer ($z^* \in [0, 0.5]$) vertical fluctuations are in fact amplified ($\phi > 1$). This helps explain the shape of $J$ in strong FST. By symmetry, our FST flow statistics will satisfy $\overline{uu} = \overline{vv}$ and $\overline{uv} = 0$, from which one can show that

$$J = \frac{1}{4}\,\phi\,(3-\phi)^2. \tag{5.3}$$

We note that, due to finite sample sizes, measurements will satisfy (5.3) approximately, rather than exactly. Figure 5($c$) shows that the local minimum in $J$ at $z^* \approx -0.25$ is because this is where vertical fluctuations are most suppressed. In the upper surface layer, figure 5($c$) shows that amplification of vertical fluctuations is strongest at $z^* \approx 0.3$. While less pronounced than the local minimum at $z^* \approx -0.25$, we do see for the larger $Fr_T^2$ in figure 5($b$) evidence of a local minimum in $J$ at $z^* \approx 0.3$. For $\phi$ to go from $<1$ in the lower surface layer to $>1$ in the upper surface layer, it must pass through $\phi = 1$ around the mean free surface. This explains why near-perfect isotropy ($J \approx 1$) is observed at the mean free surface ($z^* = 0$) for strong FST in figure 5($b$).

### 5.2. *Momentum*

We now examine the vertical momentum equation. We define density fluctuations $\rho' \equiv \rho - \overline{\rho}$, in which case the vertical component of (3.1$a$) is

$$\frac{\partial \rho w}{\partial t} = -\boldsymbol{\nabla}\boldsymbol{\cdot}\,(\boldsymbol{u}\rho w) - \partial p_d/\partial z + \partial \tau_{i3}/\partial x_i + \rho' g, \tag{5.4}$$

where dynamic pressure $p_d$ is the total pressure minus a reference pressure $p_0$ and hydrostatic pressure:

$$p_d \equiv p - p_0 - g\int_z^\infty \overline{\rho}\,\mathrm{d}z'. \tag{5.5}$$

Averaging (5.4) and splitting Reynolds stress into two terms $\overline{\rho ww} = \overline{\rho}\;\overline{ww} + \overline{\rho' ww}$, we are left with the derivative of four momentum flux terms:

$$0 = -\frac{\partial}{\partial z}\left(\overline{\rho}\;\overline{ww} + \overline{\rho' ww} + \overline{p_d} - \overline{\tau_{33}}\right). \tag{5.6}$$

The appropriate choice of $p_0$ makes the sum of momentum flux terms zero.

In figure 7 we plot (per unit mass) the mean-density component of Reynolds stress $\overline{ww}$, the fluctuating-density component of Reynolds stress $\overline{\rho' ww}/\overline{\rho}$ and the viscous stress $-\overline{\tau_{33}}/\overline{\rho}$. Pressure stress $\overline{p_d}/\overline{\rho}$ cancels the sum of these three stresses. We see that plotting against $z^*$ and normalising the stresses by $u_{rms}^2$ measured at the bottom of the surface layer ($z^* = -0.5$) does a reasonable job in collapsing the results, and makes clear the distinct behaviour between strong and moderate FST. Beneath the surface layer ($z^* < -0.5$), there is no contribution from the fluctuating-density component of Reynolds stress or viscous stress. Within the surface layer, viscous stress is of order $Re_T^{-1}$, meaning it is negligible in this DNS and certainty negligible at larger $Re_T$ typical of real-world FST. For strong FST, we see that $\overline{ww}$ slightly decreases in the lower surface layer as vertical fluctuations are suppressed, then slightly increases in the upper surface layer as vertical fluctuations are amplified, consistent with figure 5($c$).

We now focus on the fluctuating-density component of Reynolds stress $\overline{\rho' ww}$. Within the lower surface layer this term becomes slightly negative, then increases through the upper surface layer. As with intermittency in § 4.1, we can split this term into separate contributions from bubbles, droplets and the free surface. Recalling (3.2),



https://doi.org/10.1017/jfm.2026.11535 Published online by Cambridge University Press

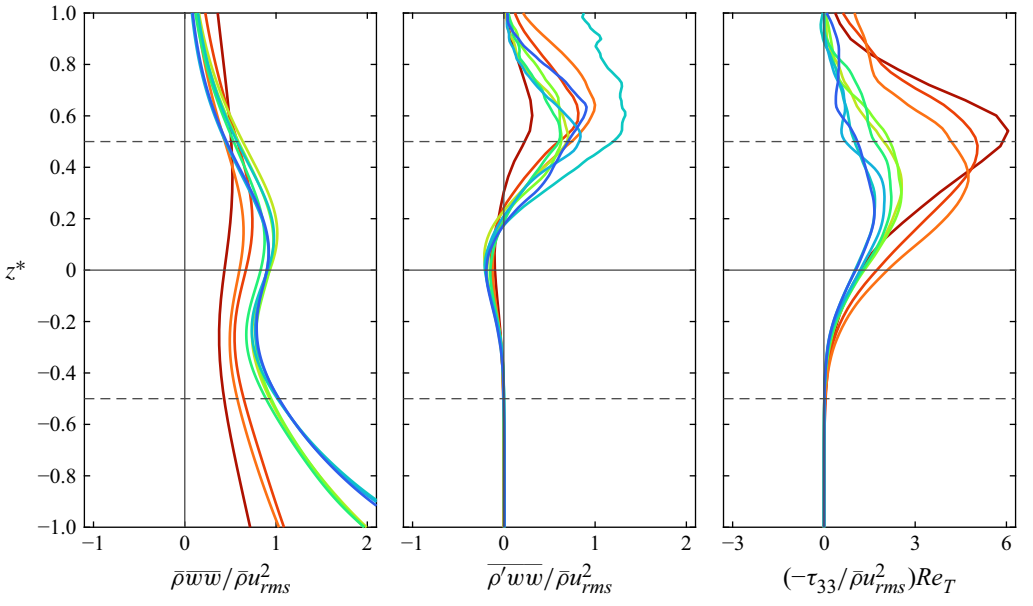



Figure 7. Momentum flux across a range of $Fr_T^2$ (see figure 1*a* for colour legend), normalised by mean density $\overline{\rho}$ measured for each $z^*$ and characteristic velocity $u_{rms}$ measured at $z^* = -0.5$ (see table 1). For the viscous term, we further multiply by $Re_T$ to bring it to a similar scale.

we can write density fluctuations as $\rho' = \Delta\rho(c - \gamma)$, where $\Delta\rho = \rho_w - \rho_a$. Thus, the density fluctuations caused by the free surface can be obtained by $\rho_0' \equiv \Delta\rho(c_0 - \gamma_0)$, and similar for $\rho_B'$ describing fluctuations caused by bubbles and $\rho_D'$ describing fluctuations caused by droplets. This allows us to decompose $\overline{\rho' ww}$ into these three terms:

$$\overline{\rho' ww} = \overline{\rho_0' ww} + \overline{\rho_B' ww} + \overline{\rho_D' ww}, \tag{5.7}$$

shown in figure 8. We see that, by at least two orders of magnitude, the free-surface effect ($\overline{\rho_0' ww}$) dominates bubble or droplet effects. As one might expect, droplets only have a (small) effect above the mean free surface ($z^* = 0$). Bubbles, on the other hand, never have a significant effect through $\overline{\rho_B' ww}$, even for larger $Fr_T^2$ where the void fraction is larger. To explain these features, we note that $-\overline{\rho_B' ww}$ can be interpreted as the correlation between the presence of a bubble ($\rho_B' < 0$) and large vertical velocities ($ww > \overline{ww}$). Zero correlation is what one would obtain if bubbles were treated as passive particles, showing that, for the $Fr_T^2$ considered here, bubbles are primarily advected by turbulence, with buoyancy having a smaller contribution.

### 5.3. *Turbulence kinetic energy*

We now examine the turbulence kinetic energy equation. Taking the inner product of (3.1*a*) and $\boldsymbol{u}$:

$$\frac{\partial}{\partial t}\left(\frac{1}{2}\rho\boldsymbol{u}\cdot\boldsymbol{u}\right) = -\boldsymbol{\nabla}\cdot\left[\boldsymbol{u}\left(\frac{1}{2}\rho\boldsymbol{u}\cdot\boldsymbol{u}\right) + \boldsymbol{u}p - \boldsymbol{u}\cdot\boldsymbol{\tau}\right] - \boldsymbol{\tau} : \boldsymbol{\nabla}\boldsymbol{u} - g\rho w. \tag{5.8}$$

To obtain the governing equation for $\overline{\rho}\tilde{k}$, we take the average. Noting that the averaged conservation of mass equation gives $\overline{\rho w} = 0$, the gravity term cancels and we have

$$0 = -\frac{\partial}{\partial z}\left(\frac{1}{2}\overline{\rho w u_i u_i} + \overline{wp} - \overline{u_i \tau_{i3}}\right) - \overline{\rho}\varepsilon. \tag{5.9}$$



https://doi.org/10.1017/jfm.2026.11535 Published online by Cambridge University Press

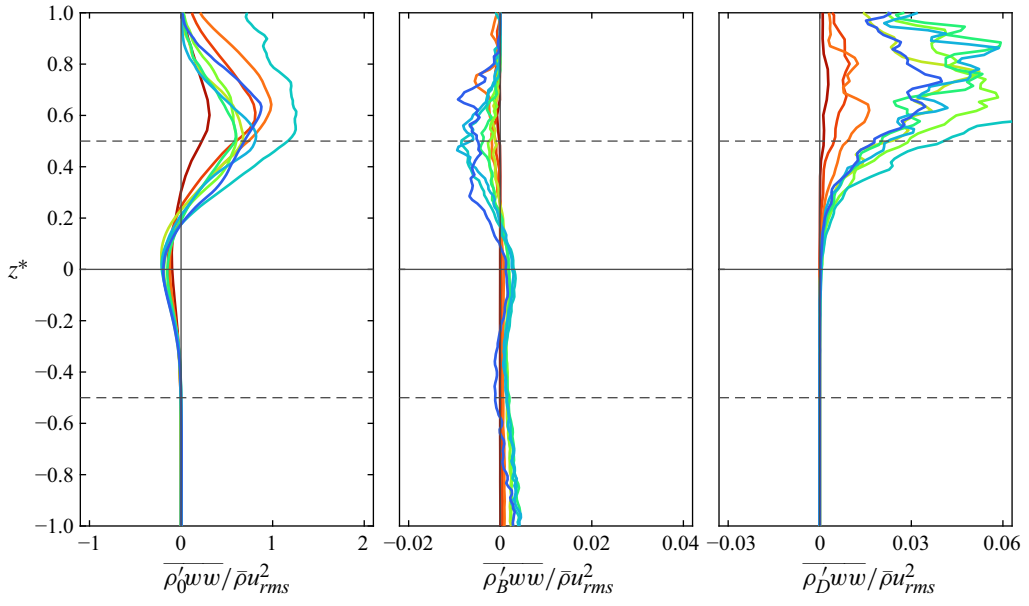



Figure 8. Components of $\overline{\rho' ww}$ from (5.7), normalised by mean density $\overline{\rho}(z^*)$ and characteristic velocity $u_{rms}$ measured at $z^* = -0.5$ (see table 1) across a range of $Fr_T^2$ (see figure 1*a* for colour legend).

In § 5.3.1 we compare the evolution of $\tilde{k}$ and $\varepsilon$ between the simulations with the free surface and single-phase simulation to show, especially for strong FST, that free-surface effects are restricted to within the surface layer. In § 5.3.2 we examine $\tilde{k}$ and $\varepsilon$ within the surface layer. In § 5.3.3 we focus on the energy flux terms in (5.9). Predicting the flux of energy into the surface layer will form an important part of the turbulence model discussed in § 6.

### 5.3.1. *Extent of the effect of the free surface on turbulence*

Recall that our simulation set-up injects turbulence kinetic energy $\tilde{k}$ in a region deep beneath the free surface, which then diffuses towards the surface, while some energy is dissipated by $\varepsilon$. Because of this set-up, turbulence levels vary with depth, even in the absence of free-surface effects (Guo & Shen 2009). To elucidate the effect of the free surface on $\tilde{k}$ and $\varepsilon$, we first perform a new DNS without any free surface. This simulation has the same set-up as the air–water simulations described in § 3, except the entire domain is filled with water. We find that placing the upper boundary at $z = \pi$ (leading to the same domain size as that of the air–water simulations with an air gap of $\pi$) is sufficient such that the upper boundary has negligible effect on the turbulence at $z = 0$ (the location of the quiescent free surface in the other simulations).

Figure 9 compares $\tilde{k}$ and $\varepsilon$ from the simulations with a free surface and the new simulation without a free surface. Turbulence values are normalised by the value at $z = -\pi/2$, the depth above which there is no forcing and the flow evolves naturally. Focusing first on figures 9(*a*) and 9(*c*), in the absence of the free surface we see the expected exponential decay of both $\tilde{k}$ and $\varepsilon$ with decreasing depth (Guo & Shen 2009). This is also true for simulations with the free surface at deeper depths; however, at shallower depths both $\tilde{k}$ and $\varepsilon$ depart and are much larger than in the absence of the free surface.



https://doi.org/10.1017/jfm.2026.11535 Published online by Cambridge University Press

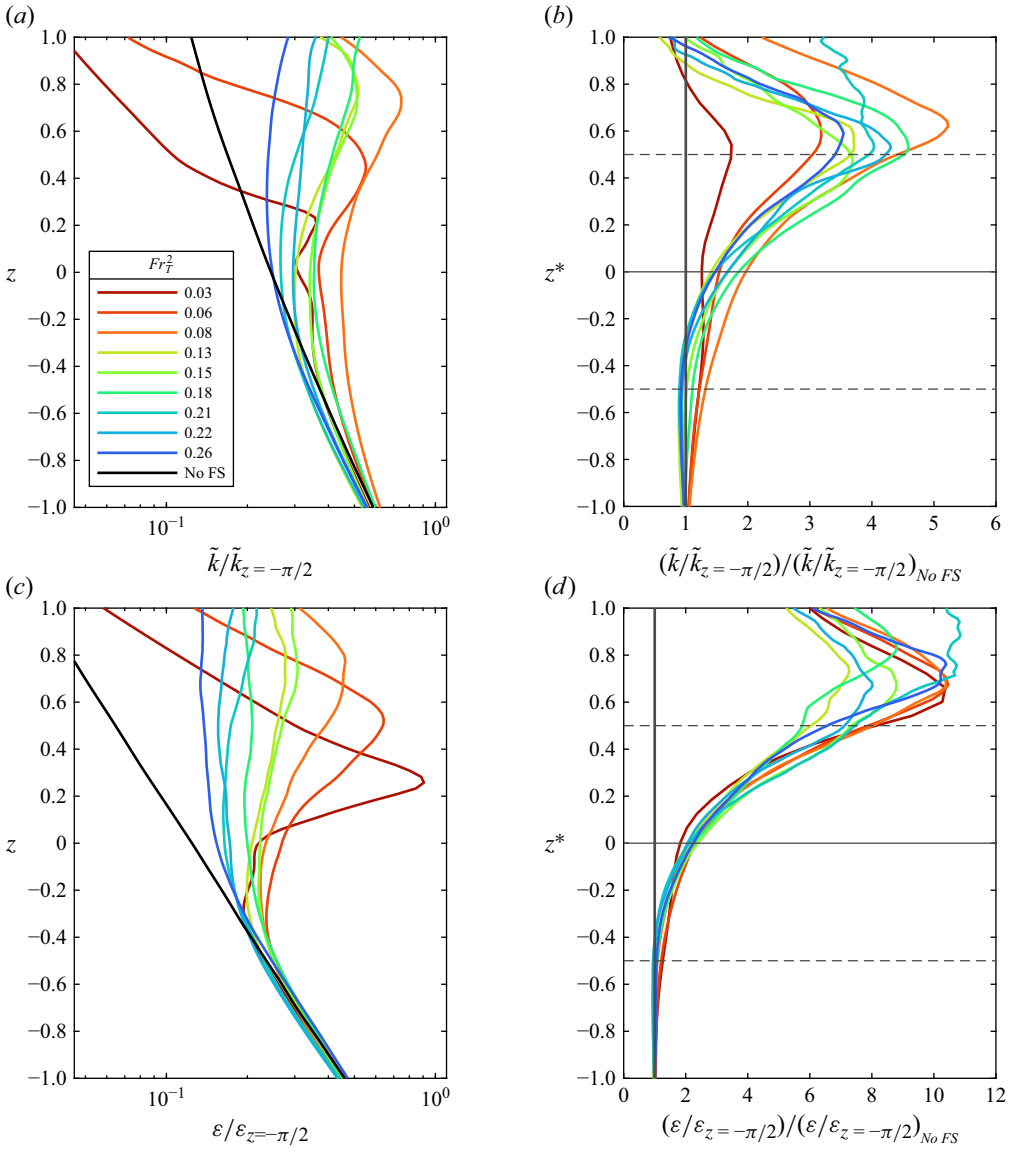



Figure 9. (*a*,*b*) Turbulence kinetic energy $\tilde{k}$ and (*c*,*d*) dissipation rate $\varepsilon$ across a range of $Fr_T^2$ (see figure 1*a* for colour legend), compared with a simulation without a free surface (solid black line).

To quantify the amplification of $\tilde{k}$ and $\varepsilon$ due to the free surface, in figures 9(*b*) and 9(*d*) we compare the value of $\tilde{k}$ and $\varepsilon$ in simulations with the free surface to the value at the same $z$ in the simulation without the free surface. We then normalise and plot in terms of $z^*$. While there are some small variations beneath, we see that, especially for strong FST, significant amplification of $\tilde{k}$ and $\varepsilon$ only happens within and above the surface layer ($z^* > -0.5$). These results demonstrate that the free surface does not directly affect the turbulence beneath the surface layer, and that $z^* = -0.5$ is an appropriate definition of the lower limit of the surface layer. This would suggest that outside of the surface layer standard turbulence closure models are applicable; however, within the surface layer a model must account for the free-surface effects, namely an increase of $\tilde{k}$ by as much as a



https://doi.org/10.1017/jfm.2026.11535 Published online by Cambridge University Press

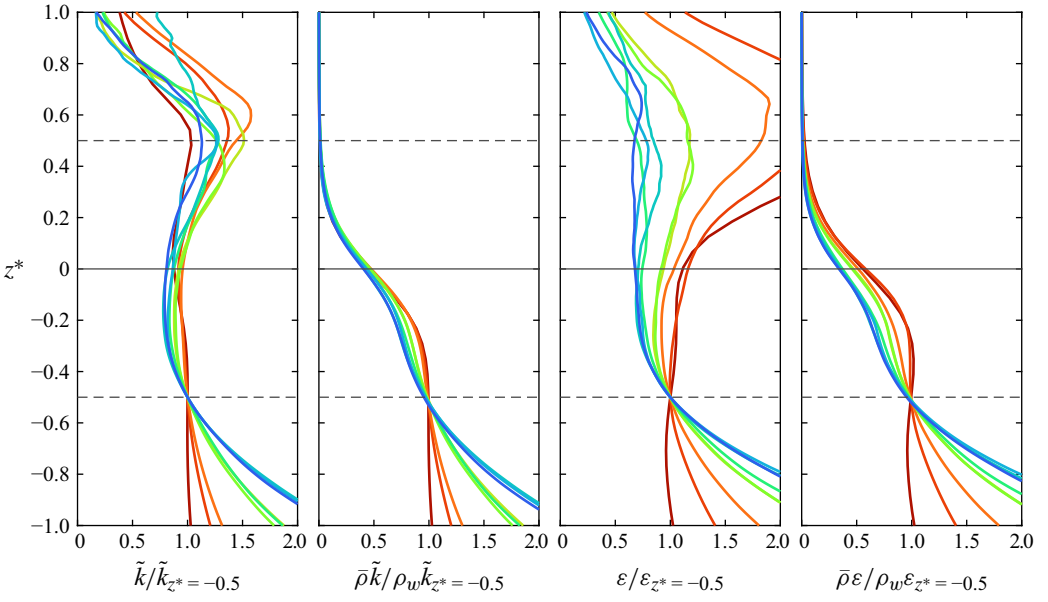



Figure 10. Turbulence kinetic energy $\tilde{k}$ and dissipation rate $\varepsilon$, per unit volume and per unit mass across a range of $Fr_T^2$ (see figure 1*a* for colour legend).

factor of 5 and $\varepsilon$ by as much as a factor of 10 relative to flow without a free surface, as seen in figures 9(*b*) and 9(*d*), respectively.

### 5.3.2. *Turbulence within the surface layer*

We now consider the turbulence levels within the surface layer, shown in figure 10. For the turbulence kinetic energy per unit mass $\tilde{k}$, we see that there is relatively little variation within the surface layer, especially for the lower surface layer ($z^* \in [-0.5, 0]$); throughout the surface layer, $\tilde{k}$ does not depart significantly from the value at the bottom of the surface layer ($z^* = -0.5$). Furthermore, due to $\rho_a \ll \rho_w$ the small variation in the upper surface layer ($z^* \in [0, 0.5]$) is negligible when one considers the turbulence kinetic energy per unit volume, $\overline{\rho}\tilde{k}$.

For the turbulent dissipation rate per unit mass $\varepsilon$, the variations in the surface layer are slightly larger than for $\tilde{k}$, but still $\varepsilon$ measured at the bottom of the surface layer does a good job in characterising dissipation rates within the surface layer, especially the lower surface layer ($z^* \in [-0.5, 0]$). Because $\rho_a \ll \rho_w$ the majority of the dissipation of energy happens in the lower surface layer. For turbulent dissipation rate per unit volume, $\overline{\rho}\varepsilon$, we see a strong collapse for $Fr_T^2 > 0.2$, and note that the transition towards this behaviour begins around $Fr_T^2 = 0.1$.

### 5.3.3. *Energy flux into the surface layer*

We now investigate the three energy flux terms in (5.9), shown in figure 11. Similar to the momentum flux terms, we plot against $z^*$ and normalise the stresses by $u_{rms}^3$ measured at the bottom of the surface layer ($z^* = -0.5$). First, we note that, as expected, the viscous diffusion term $\overline{u_i \tau_{i3}}$ is of order $Re_T^{-1}$, meaning it is negligible in this DNS and certainly negligible at larger $Re_T$ typical of real-world FST. For the remaining terms, we see turbulent diffusion $\overline{\rho w u_i u_i}$ moves energy upward into the surface layer, and pressure



https://doi.org/10.1017/jfm.2026.11535 Published online by Cambridge University Press

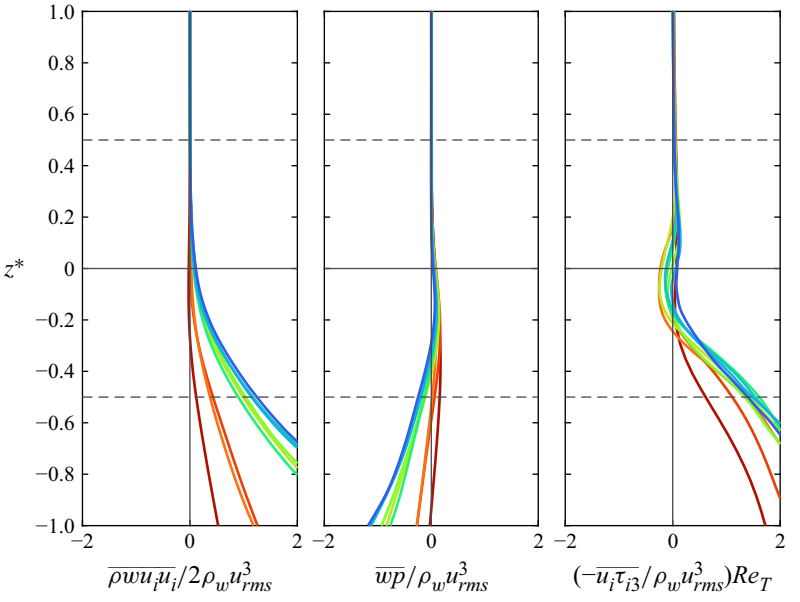



Figure 11. Turbulence kinetic energy flux terms across a range of $Fr_T^2$ (see figure 1*a* for colour legend), normalised by water density $\rho_w$ and characteristic velocity $u_{rms}$ measured at $z^* = -0.5$ (see table 1). For the viscous term, we further multiply by $Re_T$ to bring it to a similar scale.

diffusion $\overline{wp}$ partially counteracts this, moving some energy out of the surface layer. Of note, despite scaling by $z^*$ and $u_{rms}$, we still see $Fr_T^2$ dependence in these energy flux terms.

While we have shown that the turbulence beneath the surface layer does not directly feel the free surface, the increased energy dissipation within the surface layer is still important to the overall energy budget of the flow. Thus, the energy flux into the surface layer (i.e. the net work done on the surface layer by the turbulence beneath) is an important quantity for any closure model. This net work is given by the sum of turbulent, pressure and viscous diffusion measured at the bottom of the surface layer:

$$W = \left[\frac{1}{2}\overline{\rho w u_i u_i} + \overline{wp} - \overline{u_i \tau_{i3}}\right]_{z^*=-0.5}. \tag{5.10}$$

Because the viscous term is negligible in this DNS and certainly negligible at larger $Re_T$ typical of real-world FST, we consider

$$W \approx \left[\frac{1}{2}\overline{\rho w u_i u_i} + \overline{wp}\right]_{z^*=-0.5}. \tag{5.11}$$

In figure 12 we show the net work non-dimensionalised by $\rho_w$ and $u_{rms}$ measured at $z^* = -0.5$. We start by considering a linear scaling with $Fr_T^2$. Linear regression gives

$$W/(\rho_w u_{rms}^3) = C_W\, Fr_T^2, \tag{5.12}$$

where the 95 % confidence interval is $C_W = 4.6 \pm 0.8$. To avoid overfitting we stick to this linear model, but note that the relatively low $R^2 = 0.641$ and some indication of a split at $Fr_T^2 = 0.1$ suggest some improvement could be possible with additional simulations. Dimensionalising, we see how the work done on the surface layer depends on gravity and



https://doi.org/10.1017/jfm.2026.11535 Published online by Cambridge University Press

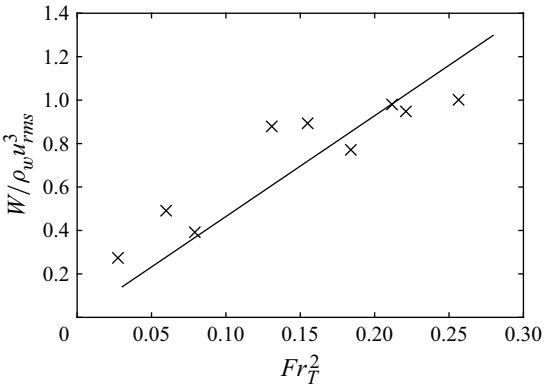



Figure 12. Work done on the surface layer by turbulence beneath (5.11) as a function of $Fr_T^2$. The solid line shows the linear fit to (5.12) with $C_W = 4.6$ ($R^2 = 0.641$).

the turbulence ($\varepsilon$ and $u_{rms}$) measured at the bottom of the surface layer:

$$W/\rho_w = C_W\, u_{rms}^2 \varepsilon g^{-1}. \tag{5.13}$$

While this described the $Fr_T^2 \in [0.03, 0.3]$ we consider, we note that (5.13) is not expected to apply to weak FST ($Fr_T^2 \ll 1$), where near-surface turbulence is strongly affected by viscosity (Shen *et al.* 1999).

## 6. Surface-layer boundary conditions for RANS

We have shown that, particularly for strong FST, there is a clear difference between the turbulence beneath the surface layer and the turbulence within the surface layer, with $z^* = -0.5$ doing a good job in separating the two. Because the turbulence beneath the surface layer is not directly affected by the free surface, standard RANS closure models will likely still be appropriate there. One approach then is to model the (indirect) effects of the surface layer through a boundary condition applied at $z^* = -0.5$ (dimensionalised, $z = \bar{\eta} - \delta_s/2$), analogous to wall models for boundary layers.

We first need $\delta_s$ to know where to apply this boundary condition. So far, we have obtained the surface-layer thickness $\delta_s$ *a posteriori* using measurements of $\gamma(z)$, as described by (2.6). For a predictive model appropriate to RANS, we need to be able to predict $\delta_s$ based on the turbulence levels $\varepsilon$ and $u_{rms}^2 = 2\tilde{k}/3$. Figure 13 shows the scaling of $\delta_s$, normalised by the characteristic turbulence length scale $\ell = u_{rms}^3/\varepsilon$, as a function of $Fr_T^2$. We see a strong linear relationship:

$$\delta_s/\ell = C_\delta\, Fr_T^2, \tag{6.1}$$

where the 95 % confidence interval is $C_\delta = 11.1 \pm 1.1$. Dimensionalising:

$$\delta_s = C_\delta\, u_{rms}^2 g^{-1}. \tag{6.2}$$

This is the scaling one would expect from a simple wave argument: that energy is roughly evenly distributed between gravitational potential energy ($\propto \rho_w g \delta_s$) and kinetic energy ($\propto \rho_w u_{rms}^2$). We note that $u_{rms}$ is measured at $z^* = -0.5$, which is a function of $\delta_s$. This makes (6.2) an implicit equation, but because $u_{rms}$ changes smoothly with depth (see $\tilde{k}$ in figure 10), solving (6.2) should not be a challenge.



https://doi.org/10.1017/jfm.2026.11535 Published online by Cambridge University Press

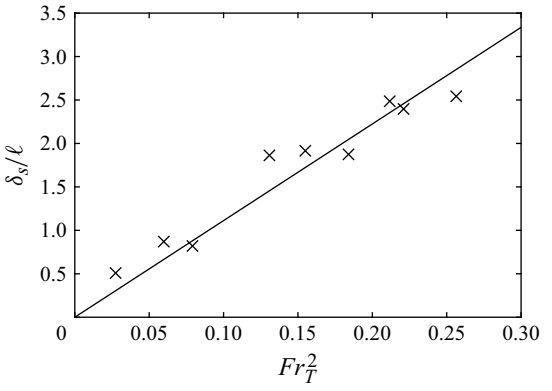



Figure 13. Surface-layer thickness $\delta_s$ normalised by the characteristic length scale $\ell = u_{rms}^3/\varepsilon$ measured at $z^* = -0.5$, as a function of $Fr_T^2$. The solid line shows the linear fit to (6.1) with $C_\delta = 11.1$ ($R^2 = 0.909$).

For a $k$–$\varepsilon$ RANS model, we need to apply a boundary condition to the turbulence kinetic energy transport equation. This boundary condition describes the flux of turbulence kinetic energy across the surface-layer boundary at $z^* = -0.5$. Brocchini (2002) derived the form of this boundary condition for free-surface flows in general, which could include turbulent energy production by mean shear within the surface layer. In our horizontally and temporally homogeneous simulations, energy flux is only driven by turbulent dissipation within the surface layer. This flux of $\tilde{k}$ into the surface layer (per unit area) is given by (5.13). Using (6.2), we can rewrite (5.13) as

$$W/\rho_w = (C_W/C_\delta)\,\varepsilon\,\delta_s. \tag{6.3}$$

While Brocchini (2002) considers $k = \overline{\boldsymbol{u}\cdot\boldsymbol{u}}/2$ rather than $\tilde{k} = \overline{\rho\boldsymbol{u}\cdot\boldsymbol{u}}/2\overline{\rho}$, beneath the surface layer $\gamma \approx 1$ and the difference should be negligible. Therefore, this $C_W/C_\delta = 0.41$ is equivalent to $C_{diss}$ discussed by Brocchini (2002, (34)).

Finally, while we calculate the energy flux across the surface-layer boundary directly, if we assume that dissipation in air is negligible (vacuum assumption), it could also be determined based on the integral of dissipation (Brocchini 2002; Iravani *et al.* 2020):

$$W/\rho_w \approx \delta_s \int_{-0.5}^{0.5} \varepsilon\gamma \,\mathrm{d}z^*. \tag{6.4}$$

Recalling figure 10, as a first approximation one could model the dissipation rate per unit mass in the surface layer as a constant equal to $\varepsilon$ measured at $z^* = -0.5$. Using any distribution of $\gamma$ where $\gamma - 0.5$ is symmetric about $\bar{\eta}$ (this includes both the Gaussian (2.5) and logistic (4.3) distributions), we obtain $W/\rho_w \approx 0.5\varepsilon\,\delta_s$, or $C_W/C_\delta \approx 0.5$. For comparison, we also consider dissipation decreasing linearly to zero at the top of the surface layer, as assumed by Iravani *et al.* (2020). In that case, (6.4) gives $C_W/C_\delta \approx 0.361$ if one uses (2.5) for $\gamma$ and $C_W/C_\delta \approx 0.329$ if one uses (4.3) for $\gamma$. Thus, our directly measured $C_W/C_\delta = 0.41 \approx 0.5$ is consistent with the simplified description of dissipation being constant in the surface layer, although the difference if one assumed linearly decreasing dissipation is not too large.

## 7. Conclusion

For sufficiently large $Fr_T^2$, turbulence is strong enough to overcome the restoring force of gravity and break apart the free surface, leading to air entrainment. Our interest is



https://doi.org/10.1017/jfm.2026.11535 Published online by Cambridge University Press

characterising the turbulence in the resulting surface layer, where air and water are highly mixed. The turbulence in this region drives bubble evolution mechanisms, but it is hard to predict using turbulence modelling, like RANS.

We develop a definition of the surface-layer thickness $\delta_s$ based on the derivative of intermittency $\mathrm{d}\gamma/\mathrm{d}z$ at the mean free-surface height $z = \bar{\eta}$. This removes dependence of $\delta_s$ on the tail behaviour of $\gamma$, which can be affected by the ($Fr_T^2$-dependent) bubble void fraction deep beneath $\bar{\eta}$ and makes no assumptions about the distribution of $\gamma$. We find this robust definition of the surface layer is appropriate to characterise the relevant properties of the near-surface turbulence. In particular, scaling depth by $z^* = (z - \bar{\eta})/\delta_s$ collapses results across broad ranges of $Fr_T^2$, and there is a clear difference in behaviour between within the surface layer and beneath the surface layer, separated by $z^* = -0.5$.

We show the collapse with $z^*$ for intermittency, turbulence isotropy, turbulent momentum flux and turbulent energy flux. For intermittency, we show that even at $Fr_T^2$ as large as 0.26 the surface-layer intermittency is driven by the movement of a mostly intact free surface (rather than bubbles or droplets), and that the distribution is better modelled as logistic, rather than Gaussian as often assumed (Brocchini & Peregrine 2001*b*). For isotropy, scaling by $z^*$ provides strong evidence that the transition to strong FST (defined here as turbulence strong enough such that nearly isotropic turbulence is obtained in the surface layer) happens around $Fr_T^2 \approx 0.1$, as first suggested by Gaylo & Yue (2025). Our measurements of turbulence highlight that, particularly for strong FST, the direct modification of near-surface turbulence is primarily due to the intermittency of the free surface (as opposed to bubbles or droplets), and that it is constrained to the surface layer ($z^* \in [-0.5, 0.5]$). We show that the resulting turbulence within the surface layer follows a universal behaviour characterised by $\delta_s$ as well as $\varepsilon$ and $u_{rms}$ measured at the bottom of the surface layer ($z^* = -0.5$).

In § 6 we discuss that, because the direct effects of the free surface are largely constrained to the surface layer, RANS turbulence modelling could be applied without modification beneath the surface layer, with a boundary condition at the bottom of the surface layer capturing the indirect effects though energy flux. This is similar to the thin-layer model theorised by Brocchini (2002). We determine the scaling of $\delta_s$ and the energy flux into the surface layer, $W$, with $Fr_T^2$, and linear regression to DNS data provides the scaling: $\delta_s \approx 11.1\, u_{rms}^2 g^{-1}$ and $W \approx 0.41\, \varepsilon \delta_s$. These are the two relationships needed to implement a surface-layer boundary condition in $k$–$\varepsilon$ RANS modelling. Our model applies directly to FST where a significant separation in scales makes near-surface turbulence independent of the specific turbulence-generating mechanism beneath the surface, which also establishes a foundation on which models for other free-surface flows can be developed.

**Acknowledgements.** The authors thank Dr K. Hendrickson for collaboration on the DNS solver.

**Funding.** This work was funded by the US Office of Naval Research (grant number N00014-24-1-2076) under the oversight of Dr W.-M. Lin and Dr Y.L. Young. The computational resources were funded through the Department of Defense High Performance Computing Modernization Program.

**Declaration of interests.** The authors report no conflict of interest.

## References

Brocchini, M. 2002 Free surface boundary conditions at a bubbly/weakly splashing air–water interface. *Phys. Fluids* **14** (6), 1834–1840.

Brocchini, M. & Peregrine, D.H. 1996 Integral flow properties of the swash zone and averaging. *J. Fluid Mech.* **317**, 241–273.



https://doi.org/10.1017/jfm.2026.11535 Published online by Cambridge University Press

BROCCHINI, M. & PEREGRINE, D.H. 2001*a* The dynamics of strong turbulence at free surfaces. Part 1. Description. *J. Fluid Mech.* **449**, 225–254.

BROCCHINI, M. & PEREGRINE, D.H. 2001*b* The dynamics of strong turbulence at free surfaces. Part 2. Free-surface boundary conditions. *J. Fluid Mech.* **449**, 255–290.

CALADO, A. & BALARAS, E. 2025 Interfacial deformation and energy exchange in free-surface turbulence. *J. Fluid Mech.* **1025**, A52.

CAMPBELL, B. 2014 A mechanistic investigation of nonlinear interfacial instabilities leading to slug formation in multiphase flows. PhD thesis, MIT.

CHANSON, H. 1996 *Air Bubble Entrainment in Free-Surface Turbulent Shear Flows*. Academic Press.

GAYLO, D.B. & YUE, D.K.P. 2025 Size distribution of large air bubbles entrained by strong free-surface turbulence. *J. Fluid Mech.* **1020**, A40.

GUO, X. & SHEN, L. 2009 On the generation and maintenance of waves and turbulence in simulations of free-surface turbulence. *Comput. Fluids* **228** (19), 7313–7332.

GUO, X. & SHEN, L. 2010 Interaction of a deformable free surface with statistically steady homogeneous turbulence. *J. Fluid Mech.* **658**, 33–62.

HENDRICKSON, K., WEYMOUTH, G.D., YU, X. & YUE, D.K.P. 2019 Wake behind a three-dimensional dry transom stern. Part 1. Flow structure and large-scale air entrainment. *J. Fluid Mech.* **875**, 854–883.

HENDRICKSON, K., WEYMOUTH, G.D. & YUE, D.K.P. 2020 Informed component label algorithm for robust identification of connected components with volume-of-fluid method. *Comput. Fluids* **197**, 104373.

HENDRICKSON, K. & YUE, D.K.P. 2019 Wake behind a three-dimensional dry transom stern. Part 2. Analysis and modelling of incompressible highly variable density turbulence. *J. Fluid Mech.* **875**, 884–913.

HINZE, J.O. 1955 Fundamentals of the hydrodynamic mechanism of splitting in dispersion processes. *AIChE J.* **1**, 289–295.

IRAVANI, N., BADIEI, P. & BROCCHINI, M. 2020 Novel free surface boundary conditions for spilling breaking waves. *Coast. Engng* **159**, 103717.

KILLEN, J.M. 1968 The surface characteristics of self aerated flow in steep channels. PhD thesis, University of Minnesota.

KRAMER, M. & VALERO, D. 2023 Linking turbulent waves and bubble diffusion in self-aerated open-channel flows: two-state air concentration. *J. Fluid Mech.* **966**, A37.

LUNDGREN, T.S. 2003 Linearly forced isotropic turbulence. *Tech. Rep*. Center for Turbulence Research, Stanford University.

MARTÍNEZ-BAZÁN, C., MONTAÑÉS, J.L. & LASHERAS, J.C. 1999 On the breakup of an air bubble injected into a fully developed turbulent flow. Part 1. Breakup frequency. *J. Fluid Mech.* **401**, 157–182.

POPE, S.B. 2000 *Turbulent Flows*. Cambridge University Press.

QI, Y., TAN, S., CORBITT, N., URBANIK, C., SALIBINDLA, A.K.R. & NI, R. 2022 Fragmentation in turbulence by small eddies. *Nat. Commun.* **13** (1), 469.

ROSALES, C. & MENEVEAU, C. Charles 2005 Linear forcing in numerical simulations of isotropic turbulence: physical space implementations and convergence properties. *Phys. Fluids* **17**, 095106.

RUTH, D.J., AIYER, A.K., RIVIÈRE, A., PERRARD, S. & DEIKE, L. 2022 Experimental observations and modelling of sub-Hinze bubble production by turbulent bubble break-up. *J. Fluid Mech.* **951**, A32.

RUTH, D.J. & COLETTI, F. 2024 Structure and energy transfer in homogeneous turbulence below a free surface. *J. Fluid Mech.* **1001**, A46.

SHEN, L., ZHANG, X., YUE, D.K.P. & TRIANTAFYLLOU, G.S. 1999 The surface layer for free-surface turbulent flows. *J. Fluid Mech.* **386**, 167–212.

WACLAWCZYK, T. 2021 Modeling of non-equilibrium effects in intermittency region between two phases. *Intl J. Multiphase Flow* **134**, 103459.

WEYMOUTH, G.D. & YUE, D.K.P. 2010 Conservative volume-of-fluid method for free-surface simulations on Cartesian-grids. *J. Comput. Phys.* **229** (8), 2853–2865.

WILHELMS, S.C. & GULLIVER, J.S. 2005 Bubbles and waves description of self-aerated spillway flow. *J. Hydraul. Res.* **43** (5), 522–531.

YU, X., HENDRICKSON, K., CAMPBELL, B.K. & YUE, D.K.P. 2019 Numerical investigation of shear-flow free-surface turbulence and air entrainment at large Froude and Weber numbers. *J. Fluid Mech.* **880**, 209–238.

ZABALETA, F., BOMBARDELLI, F.A. & MÁRQUEZ DAMIÁN, S. 2024 Numerical modeling of self-aerated flows: turbulence modeling and the onset of air entrainment. *Phys. Fluids* **36** (4), 043337.

https://doi.org/10.1017/jfm.2026.11535 Published online by Cambridge University Press